J. Fluid Mech. (1971), *vol.* 50, *part* 3, *pp.* 513–534
Printed in Great Britain

Autorotating wings: an experimental investigation

By E. H. SMITH
N.A.S.A. Langley Research Center, Langley, Virginia

(Received 30 October 1970 and in revised form 19 July 1971)

The autorotation of a flat plate about its spanwise axis was experimentally studied. Most of the work was done with a wing mounted in the University of Michigan 5×7 ft low-speed wind tunnel. The measurements consisted of the unsteady lift, drag, angular acceleration and the wing rotation rate. The flow pattern was studied by means of smoke, tufts and a small model in a water tunnel.

The flow pattern was very different from that over a static wing. The wing did not stall until it was nearly perpendicular to the free stream and the flow did not reattach to the lower surface until the wing had rotated well past zero angle of attack.

The maximum and average lift, drag and angular acceleration were measured for Reynolds numbers from 25 000 to 250 000. At $Re = 240\,000$ the maximum lift coefficient was 4·50 with an average value of 2·20, while the maximum drag coefficient was 4·30 with an average value of 1·60. The angular acceleration was small; the wing rotated at an almost constant angular velocity. The non-dimensional wing rotation rate was measured for Reynolds numbers from 1300 to 280 000 and approached an asymptotic limit of 0·35 for sufficiently high Reynolds numbers.

The effect of applying driving and retarding torques to the wing was studied. As the rotation rate was increased above the free autorotation rate, the lift and drag increased. When the rotation rate was reduced by a retarding torque they both decreased. The power developed by the rotating wing was considerably less than for a windmill of the same frontal area.

A variety of wing configurations were tested, including different airfoils and aspect ratios and spoilers mounted at various locations on the wing. However, except for spoilers that were so large that they prevented autorotation, none of these changes had a major effect on the gross properties of the autorotation phenomenon.

Freely falling wings were also studied. For Reynolds numbers above 4000 the average lift and drag coefficients were comparable to those observed in the fixed axis tests and it appeared that the flow pattern was similar.

1. Introduction

Autorotation is the continuous rotation, without external power, of a body exposed to an air stream. Some familiar examples of this are the windmill and cup anemometer.

The subject of this paper is a study of the autoration of a wing about its spanwise axis when it is exposed to an air stream perpendicular to that axis. This phenomenon can occur for either a wing rotating about a fixed axis or for a freely falling wing. An example of freely falling autorotation is the steady tumbling which results when a rectangular piece of stiff paper is dropped.

The autorotating wing problem is of interest at present for a number of reasons. It offers insight into the problem of dynamic stall which is an important problem in high performance helicopters and in turbine engine compressors. Also, flat plate autorotation occurs in many practical applications, such as the dropping of leaflets and the separation of panels from aircraft and spacecraft.

The autorotating wing phenomenon was studied as early as 1897 by Ahlborn and more recently by Smith (1953), Coles (1957) and others. From this work the magnitude of the average lift and drag coefficients and the wing rotation rate were known, and it was also known that autorotation is caused by lift hysteresis resulting from unsteady aerodynamic effects. However nothing was known about the flow pattern around the wing or the unsteady forces acting on it.

Since it is at present impossible to compute the flow over an autorotating wing, an experimental investigation was undertaken. This paper presents the results of that investigation. In §2 the experimental apparatus is described. In §3 the flow pattern is described and the cause of autorotation is explained. In §4 the aerodynamic forces on the wing are discussed, while the wing rotation rate is discussed in §5. In §6 the effect of a retarding torque on the wing is discussed and the behaviour of freely falling wings is discussed in §7. Finally, some conclusions about autorotation are drawn in §8.

2. Experimental apparatus

The experimental apparatus consisted of four systems. Small wings, instrumented only for measurement of rotation rate, were mounted in the University of Michigan 2×2 ft low-speed wind tunnel. A larger wing, instrumented for measurement of rotation rate, lift, drag and angular acceleration, was mounted in the University of Michigan 5×7 ft low-speed wind tunnel. A small model was mounted in a water tunnel for flow visualization. In the free fall tests, wings were dropped in various fluids and their fall observed and timed.

The first tests were conducted in the University of Michigan 2×2 ft low-speed wind tunnel. This is an open-circuit wind tunnel with the fan located downstream of the test section. It has a speed range of 1 to 68 ft/sec and the turbulence level is 0·05% at a free-stream velocity of 50 ft/sec.

The wings were flat plates of 3·1 in. chord and were from 0·02 to 0·04 chord thick. They had aspect ratios of 6·4 and 1·33 chord-diameter tip plates. They were constructed of sheet balsa with spruce or metal centre spars, as needed. The wings rotated on a simple needle bearing system. Two needles were mounted on the wing axis; the lower needle ran in a conical hole in a piece of steel mounted on the tunnel floor, while the upper needle was contained in a small metal tube (see figure 1).

The instrumented wing was used for most of the data, including all the

fixed-axis lift, drag and angular acceleration data (see figure 2). It was installed in the University of Michigan 5 × 7 ft low-speed wind tunnel. This wind tunnel is a closed-circuit single return tunnel and has a speed range of 1 to 300 ft/sec, and a turbulence level of 0·03 %.

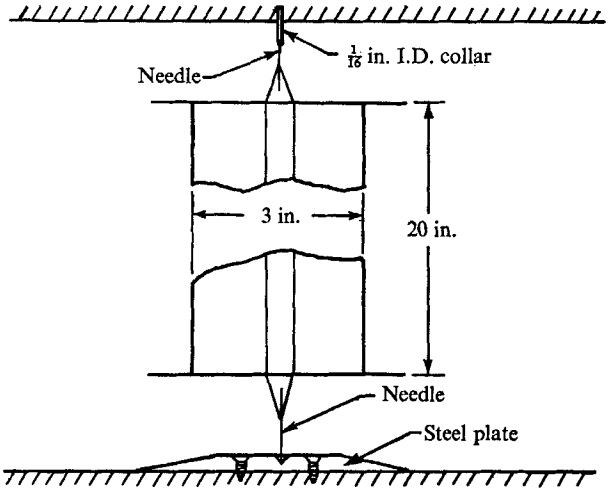

FIGURE 1. Needle bearing system for small wings.

Prior to building the instrumented wing, a number of small wings were tested in the 5 × 7 ft tunnel to determine the optimum airfoil, aspect ratio and tip plate configuration. These tests showed that the Strouhal number was nearly independent of aspect ratio, for aspect ratios greater than three, and that the best tip plate configuration was 1·33 chord-diameter tip plates fixed to the wing.† Also, the Strouhal number was relatively insensitive to airfoil shape for symmetrical airfoils. Hence the wing was built with an aspect ratio of 3·0, 1·33 chord-diameter tip plates and a 15 % thick elliptical airfoil which was symmetrical both vertically and fore and aft. The wing was constructed of balsa with a steel centre spar and had a chord of one foot.

Two bearing systems were used. The first was a pair of spherical air bearings (see figure 3). These consisted of two basic parts: the inner bearing, whose surface was the outer portion of a sphere of 4·000 in. diameter, and the outer bearing, whose inner surface was a sphere with diameter 4·004 in. The inner bearings were bolted to the wing spar while the outer bearings were bolted to a heavy steel frame mounted on the wind tunnel floor. Each outer bearing contained a plenum chamber which was connected to the bearing surface by twenty-four 0·031 in. diameter holes; these chambers were maintained at 70 psi pressure.

† The effective aspect ratio was calculated from data in Hoerner (1965) and was 5·50. The Strouhal number was reduced when the tip plates were removed or reduced in size, indicating significant tip losses. Larger plates also reduced the Strouhal number, probably because of excess drag on the rotating plates. Fixed tip plates were tested but were unsatisfactory because of air leakage through the gap even when it was as small as 0·02 chord wide.

The air bearings gave extremely low friction but their limited load capacity allowed testing up to only about $Re = 170\,000$, so a set of spherical ball bearings was used for higher speeds.

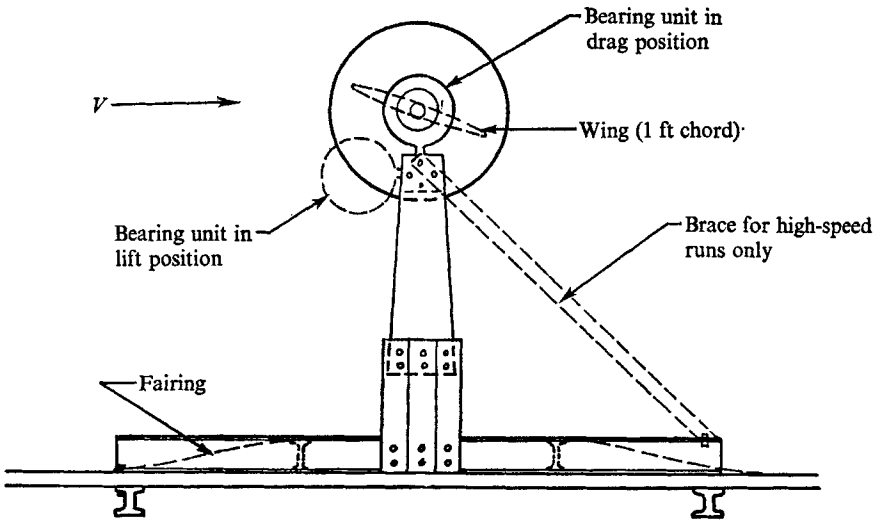

FIGURE 2. Instrumented wing apparatus in 5 × 7 ft tunnel.

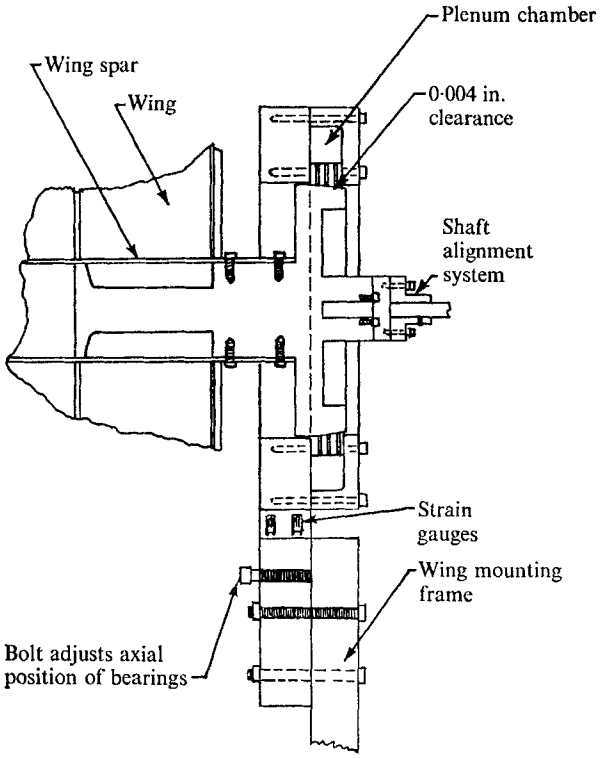

FIGURE 3. Air bearing system.

The lift and drag were measured by strain gauges mounted on a flexure cut in one of the bearing supports. These gauges were sensitive to bending only, so they measured half the drag when mounted vertically and half the lift when mounted horizontally. They were connected to a Wheatstone bridge circuit and the output was amplified and displayed on an oscilloscope. The angular acceleration was measured with a Vibrac TQ-32 optical torquemeter fitted with a flywheel to convert it into an accelerometer.

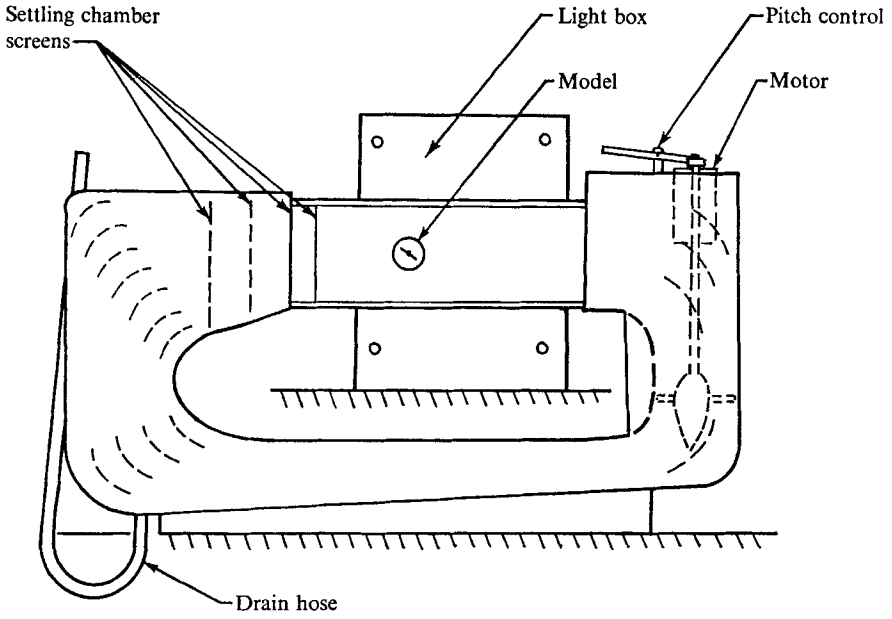

FIGURE 4. Wallis water tunnel.

The wing rotation rate was measured by a photocell system in which a photocell was mounted on one side of a tip plate and a flashlight bulb on the other. Slots were cut in the tip plate so the photocell gave a voltage pulse as each slot passed it. The pulsating signal was then amplified and fed into a digital counter. The free-stream velocity was measured with either a Pitot-static tube or a propeller anemometer.

The flow pattern was studied in the 5×7 ft tunnel with tufts attached to the wing and with smoke. The tufts furnished information at higher Reynolds numbers and were viewed by 'stopping' the wing with a strobe lamp. The smoke could only be used at low speeds but gave a better view of the flow. It was produced by putting liquid titanium tetrachloride on a rod in front of the wing or on its surface. The titanium tetrachloride then reacted with water in the air and formed a dense white smoke.

Further flow visualization work was done in the Wallis water tunnel (see figure 4). This is a small closed-circuit single return tunnel. It has a 5 in. square test section and a speed range of 0·25 to 1 ft/sec. The flow pattern is made visible by a plane of light which illuminates aluminium particles suspended in

the water. The plane of light is parallel to the flow direction and perpendicular to the wing so that it illuminates a two-dimensional plane in the flow over the wing.

The model was a small Plexiglas wing with an aspect ratio of two. It did not actually autorotate but was driven by an electric motor. Power to the motor was supplied by an auto-transformer to allow variation of the rotation rate.

Two types of tests were performed with falling wings. In the first, some of the small balsa wings used in the fixed-axis tests in the 2×2 ft tunnel were dropped in air in order to compare data for fixed-axis and freely falling autorotation. In the second series of tests, a variety of wings were dropped in air, water and a glycerol–water mixture in order to determine the range of Reynolds numbers and I^* for different types of motion.† These wings were all flat plates without tip plates. All of them had aspect ratios of 2·5 except as noted in figure 15.

Wind-tunnel tests must be corrected for the finite size of the test section. These corrections include an effective increase in the dynamic pressure caused by the reduction in test section area owing to the model and wake and changes in streamline curvature and downwash. In the autorotation tests the blockage correction was by far the largest correction. This correction was calculated by the method of Maskell (1963) for bluff bodies. This method uses the momentum equation to calculate the change in the dynamic pressure for a given amount of blockage. The method was derived for steady flow, but was assumed valid for the autorotation tests because the wing rotated rapidly enough for the vortices shed to be closely spaced. They were observed to merge quickly into a wake of relatively uniform size. The streamline curvature and downwash corrections were calculated according to data in Pope & Harper (1966) but were very small. The resulting increase in the effective dynamic pressure was large; in the 5×7 ft tunnel it increased from 31·7% of the free-stream dynamic pressure at $Re = 16\,300$ to 32·6% at $Re = 250\,000$. In the 2×2 ft tunnel the effective dynamic pressure was increased by 18·0% of the free-stream dynamic pressure.

3. The autorotation phenomenon

The unsteady flow pattern observed during autorotation is very complicated. It can be perhaps more easily understood by first considering the quasi-steady flow over a slowly rotating airfoil. Let us consider an airfoil with fore and aft symmetry rotating clockwise about a fixed axis through its mid-chord. At zero angle of attack there is no lift and no moment about the mid-chord. As the angle of attack slowly increases, a lift force, which acts at the quarter chord point, is developed; this also produces a clockwise torque about the axis of rotation. The lift and moment increase as the angle of attack increases until the wing begins to stall. As the wing stalls, the lift and moment decrease and eventually vanish when the wing is perpendicular to the free stream. Then, as the wing rotates from 90 to 180 degrees angle of attack, the process is repeated in reverse, with reversed sign on the moment and lift. At 180 degrees angle of attack the former trailing edge becomes the leading edge and the cycle repeats itself.

† I^* is the non-dimensional moment of inertia of the wing, $32I/\pi\rho c^5 A$, where I is the moment of inertia of the wing, c is its chord and A is its aspect ratio.

It is clear that the quasi-steady process described above would produce no net lift or driving torque on the wing. Therefore it could not result in autorotation because bearing friction and aerodynamic damping effects resulting from the rotation of the wing would slow the wing and eventually stop it.

In practice it was observed that a wing released from rest at an angular position at which the flow was stalled would come to rest (after a number of oscillations) in a statically stable position with the wing perpendicular to the free stream. If the wing was released at a small enough angle of attack, so that the flow was unstalled, the wing usually began autorotating and the direction of rotation corresponded to the initial direction of rotation when the wing was released. It was also observed that the wing would not autorotate if its moment of inertia was too low. The wing was then unable to store enough angular momentum to pass through the stalled portion of its cycle during which it received a retarding torque.

Hence the flow pattern over the wing obviously differed from the quasi-steady case in a manner such that the wing could gain rotational energy while the positive lift was large. The primary differences were that the wing stalled much later than in the static case and the flow reattached later to the lower surface. Thus, the positive lift and moment were increased and the negative lift and moment during the second half of the cycle were reduced. This caused the wing to increase its angular velocity further until a steady speed was reached at which the average torque was reduced to zero by aerodynamic damping effects.

The cause of the later stall of the autorotating wing was not studied in detail. However there appear to be two primary causes. The boundary layer on the upper (suction) surface of the wing takes time to thicken and separate when the angle of attack is rapidly increasing, so that the wing can reach a higher angle of attack before it stalls. Also, Ericsson & Reding (1969) pointed out that the flow over the upper surface of a wing whose angle of attack is rapidly increasing is accelerating; this reduces the adverse pressure gradient and thereby also delays the stall. The cause of the aerodynamic damping that ultimately limits the angular velocity of the wing was also not studied in detail and is not fully understood. It was observed that the lift vector acted well behind the quarter chord when the lift was large and well ahead of it during a large part of the time when the wing was stalled.

The flow pattern was studied by means of tufts and smoke in the 5×7 ft tunnel and illuminated aluminium particles in the water tunnel. Although no local velocity data were taken the flow pattern was quite clear. Figure 5 shows it for various angles of attack. Each sketch shows the instantaneous streamlines at the given angle of attack. It should be noted that these sketches show only the instantaneous streamlines outside the boundary layer, where viscous effects and the no-slip condition can be neglected. Inside the boundary layer the streamlines are complicated and very different from those shown in the sketches; no attempt was made to study the flow pattern in this region.

The lift and drag forces were also measured, with strain gauges, as a function of angle of attack. Since the autorotation problem involves an unsteady flow

field the lift is not directly proportional to the circulation as in potential flow. However, it seemed probable that the lift and circulation are still related in that when the circulation is large, the lift is large, and when the circulation is small, the lift is small. The experimental data appeared to confirm this (see figures 5 and 6). At an angle of attack of about 20°, where the lift was maximum, the

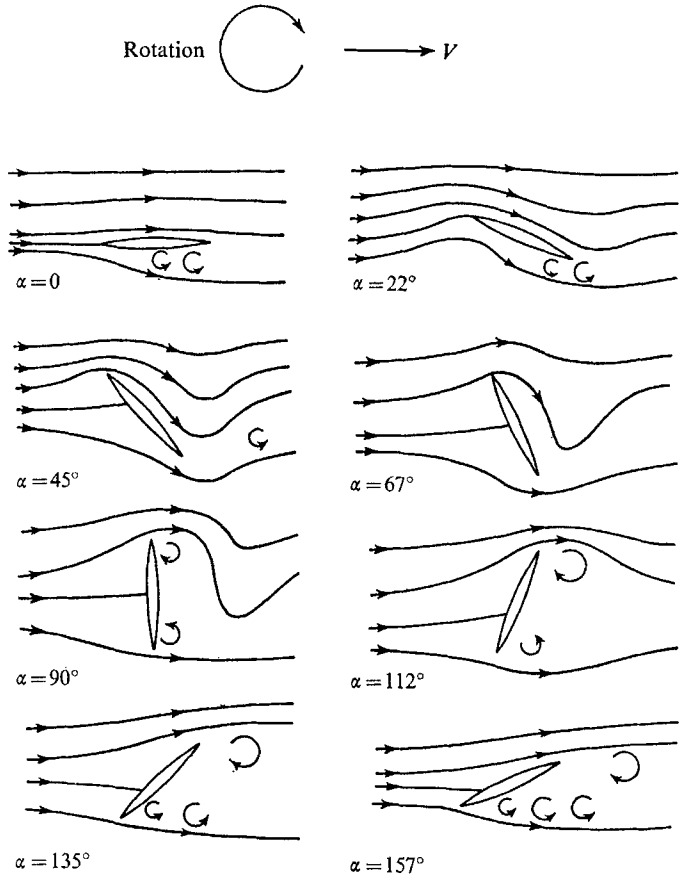

FIGURE 5. Schematic flow pattern over autorotating wing at Re = 90 000 and S = 0·35.

flow was attached and quite fast over the upper surface of the wing, while it was just attaching to the lower surface and was relatively slow there. Hence there was a large circulation around the wing. At an angle of attack of about 90°, where the lift was very small, the flow was roughly symmetrical over the front surface of the wing and was separated over the rear surface, so that the circulation was small.

The description of the flow pattern is begun at the minimum lift point, at an angle of attack of about −80°. At this point the flow had separated over the rear of the wing and the forward flow was almost stagnation flow, probably with a small net counterclockwise circulation (for flow from left to right with clockwise wing rotation). The lift was slightly negative and the drag was fairly high.

As the wing rotated, the forward stagnation point moved towards the advancing edge, with the flow becoming faster over the retreating edge and counterclockwise vorticity being shed from the leading edge. As this happened the negative lift vanished, and the lift became positive as the clockwise circulation built up. The drag decreased as the flow became faster over the retreating edge

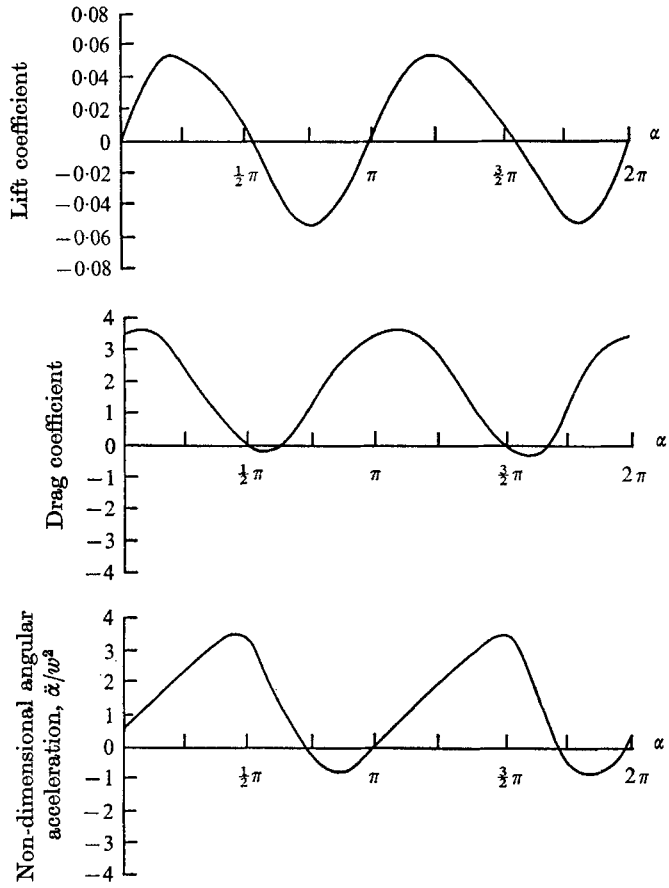

FIGURE 6. Lift and drag coefficients and non-dimensional angular acceleration *vs.* angle of attack for $Re = 90\,000$ and $S = 0{\cdot}35$.

and the pressure decreased there. At an angle of attack of about $-50°$ the drag vanished and then became negative while the lift continued to increase. The drag reached its negative peak at an angle of attack of about $-30°$ and then decreased and vanished again at about $-10°$. At an angle of attack of about 20° the flow finally began to attach to the lower surface, with the stagnation point slightly behind the leading edge. The lift levelled off as the shedding of counterclockwise vorticity from the leading edge stopped. As the angle of attack continued to increase, the flow over the upper surface remained attached while the stagnation point moved away from the leading edge on the lower surface. The drag increased rapidly, since the resultant force on the wing remained approximately constant, and its rearward component became much larger. At about 80° angle

of attack, depending on the Reynolds number, the flow began to separate, a large clockwise vortex began to form at the leading edge and a smaller counter-clockwise vortex at the trailing edge. There was a sharp peak in the drag just as the vortices were shed; this was probably an unsteady vortex-induced loading, as observed by Ham (1968).† As the two vortices, which contained the vorticity which had been producing part of the lift when it resided in the boundary layer grew and were shed, the lift and drag decreased rapidly. At an angle of attack of about $-80°$ the lift again became slightly negative to complete the cycle. Because of the rapid rotation of the wing, some of the vorticity shed from the leading edge before the flow attached to the lower surface did not have time to be carried away. Instead, it was trapped in the stagnation flow ahead of the wing and swept forward and upward and eventually carried away above the wing.

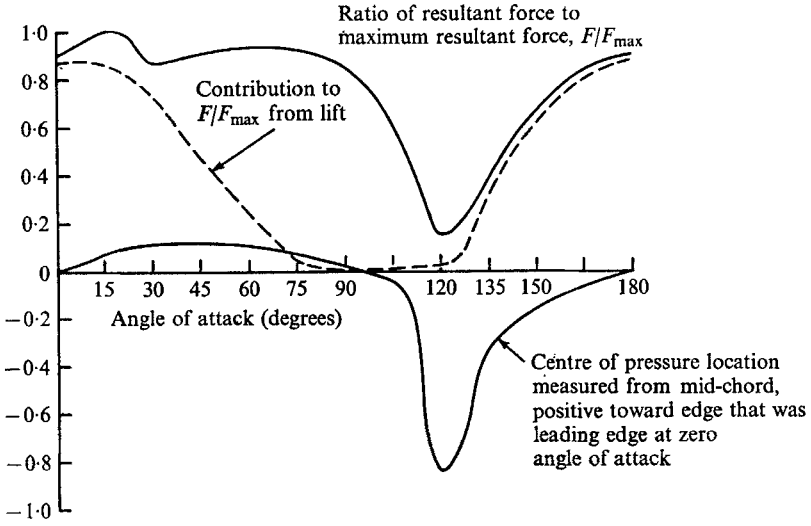

FIGURE 7. Resultant force and centre of pressure location on autorotating wing at $Re = 100\,000$, $S = 0{\cdot}35$.

The exact distribution of the lift and drag forces on the wing surface is unknown because the pressure distribution was not measured. However, it can be roughly estimated from the flow pattern and the resulting estimate of the torque agreed with the measured angular acceleration data.

The angular acceleration was zero at zero angle of attack, corresponding to the lift vector acting through the mid-chord (see figures 6 and 7). As the angle of attack increased, the forward stagnation point moved from the leading edge onto the lower surface and created a high pressure area there. This produced a driving torque and therefore positive angular acceleration, although the resultant force still acted less than 0·12 chord from the mid-chord. The angular

† N. Ham observed large lift peaks caused by vortex-induced loading during the dynamic stall of a wing at angles of attack of 20–30°, at Strouhal numbers from 0·03 to 0·12. In the autorotation tests the peak should appear as a drag peak since the stalling angle was nearly 90°.

acceleration was maximum at an angle of attack of about 35° and then began to decrease as the forward stagnation point moved toward the mid-chord. The angular acceleration vanished at an angle of attack of about 95° and then became negative. As the wing continued to rotate, the forward stagnation point moved toward the advancing edge and the flow became faster over the retreating edge. This produced a large retarding couple on the wing even though the resultant force on the wing was small at the time. The retarding moment was maximum at an angle of attack of about $-45°$ and then decreased to zero again at zero angle of attack to complete the cycle.

The most important parameters for the flow pattern were the Reynolds number and the Strouhal number S which is the wing rotation rate n in Hz non-dimensionalized by dividing it by U/c, where U is the free-stream velocity and c is the wing chord. This number can be thought of as the ratio of the time for the flow to travel one body chord length at the free-stream velocity, c/U, to the time required for the phenomenon to complete one period, $1/n$. For an autorotating wing the flow cycle repeats itself twice per wing revolution. Therefore the Strouhal number should actually be $2nc/U$, but the usual definition, nc/U, was used to avoid confusion. The ratio of the wing edge speed is given by πS, so a Strouhal number of 0·318 corresponds to the wing edge speed being equal to the free-stream velocity. For free autorotation the Reynolds number determines the Strouhal number. However, in the water-tunnel tests the Strouhal number could be varied independently of the Reynolds number, so the effect of the two parameters could be studied separately.

The Strouhal number had a strong influence on the flow pattern. As it was increased, at a given Reynolds number, the wing stalled later and the flow reattached to the lower surface later, with the stagnation point further from the edge at attachment. At low Strouhal numbers the leading edge vortex was shed well before the trailing edge vortex, but as the Strouhal number increased (at the same Reynolds number) the trailing edge vortex was shed sooner relative to the leading edge vortex and for Strouhal numbers greater than about 0·25 they were shed almost simultaneously.† As the Strouhal number was increased beyond the autorotation range the vortex shed from the leading edge became smaller and eventually disappeared. At a sufficiently high Strouhal number the flow never attached to the wing as on a static wing, but the streamlines around the wing became closed and the flow pattern away from the wing resembled that over a rotating cylinder.

The Reynolds number had a much smaller influence on the flow pattern than the Strouhal number. The flow pattern was observed for Reynolds numbers from 5000 to 90 000 and the only observed change was that at lower Reynolds numbers the wing stalled at a slightly lower angle of attack for a given Strouhal number.

† Ham (1968) studied dynamic stall of a wing starting from rest and also observed strong vortex shedding from the leading edge, with the trailing edge vortex shed later as the leading edge vortex moved back. He also observed a small vortex shed from the trailing edge just as the leading edge vortex was shed. This was not observed in the autorotation tests.

4. Aerodynamic forces

In the previous section the flow pattern was described and the relationship between the flow pattern and the unsteady aerodynamic forces was explained. This section discusses the magnitude of these forces and the influence of Reynolds number on them.

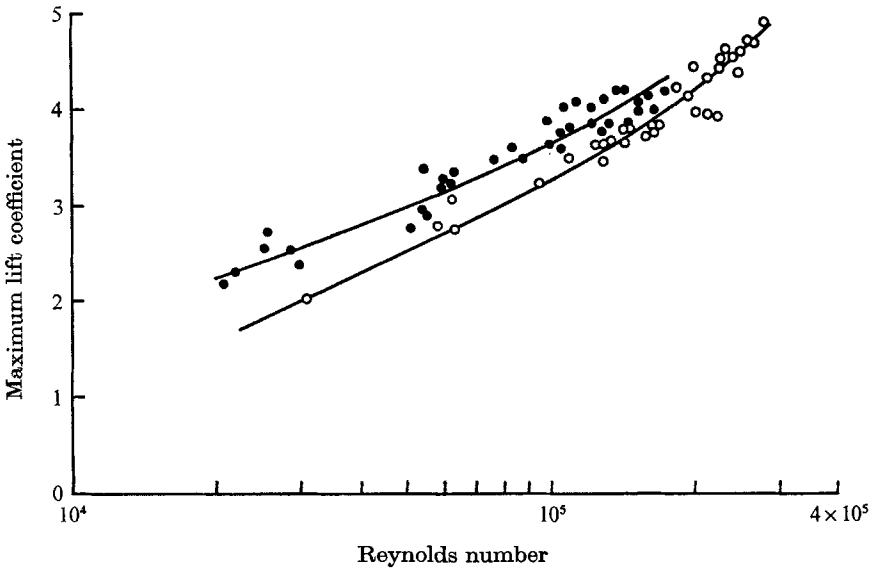

FIGURE 8. Maximum lift coefficient *vs.* Reynolds number. $I^* = 8{\cdot}47$; ○, mechanical bearings; ●, air bearings.

The unsteady aerodynamic effects discussed in §3 caused the lift and drag to be much larger than for a conventional wing in steady flow (see figures 8–10). The peak lift coefficient was 4·5 at $Re = 240\,000$, with an average value of 2·2, while the peak drag coefficient was 4·3 with an average value of 1·60. The maximum negative drag was also fairly large but the maximum negative lift was small, only about 8 % of the maximum positive lift.

The maximum and average lift and drag coefficients increased with increasing Reynolds number and were still increasing at the maximum Reynolds number tested. It would have been interesting to perform tests at higher Reynolds numbers but this was not possible because of excessive loads on the model and supports. It is expected that the lift and drag coefficients would approach an asymptotic limit at a sufficiently high Reynolds number, but this limit is unknown at present. However, it seems doubtful whether the lift and drag coefficients would become very much larger at higher Reynolds numbers, since the Strouhal number has already reached an apparent limit at about $Re = 200\,000$ (see §5). Also, the stalling angle at this Reynolds number is already about 80° and it seems unlikely that the stalling angle could become much greater than 90°.

Although the magnitude of the maximum and average lift and drag coefficients changed considerably for different Reynolds numbers, the curves of lift and

drag *vs.* angle of attack were almost unchanged. The only significant changes were that the maximum drag and minimum lift occurred slightly later and the minimum drag occurred slightly earlier at higher Reynolds numbers. The reason

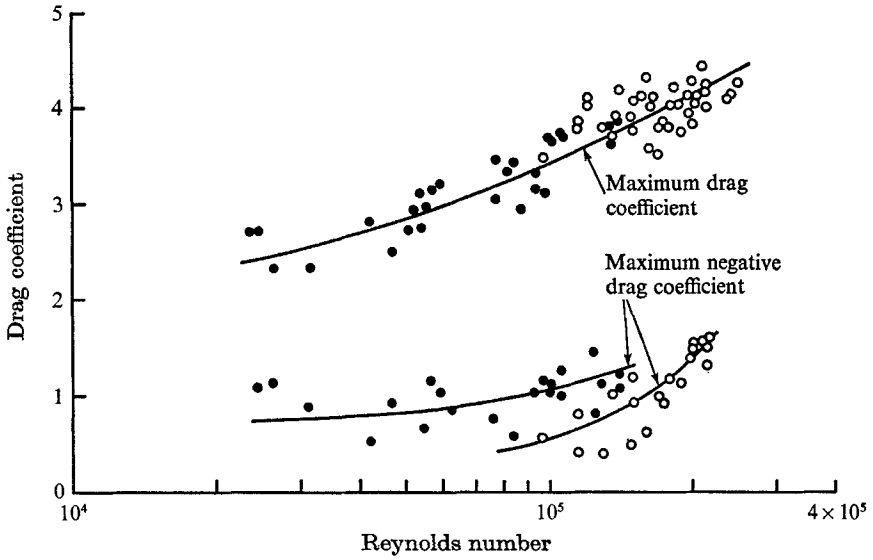

FIGURE 9. Maximum and minimum drag coefficient *vs.* Reynolds number. $I^* = 8{\cdot}47$; ○, mechanical bearings; ●, air bearings.

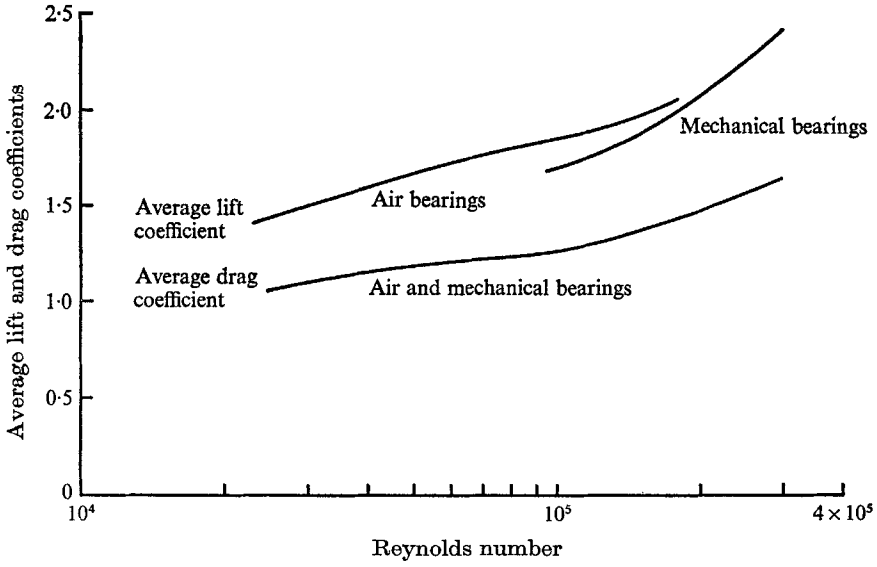

FIGURE 10. Average lift and drag coefficients *vs.* Reynolds number.

why the maximum drag and minimum lift peaks occurred later was that the wing stalled at a higher angle of attack at higher Reynolds numbers, primarily because of the higher Strouhal number (see §3). Since the wing stalled later the vortex induced loading that caused the drag peak occurred later. The vortices

were then shed later, so that the lift decreased to its minimum later. The reason why the minimum drag came earlier in the cycle at higher Reynolds numbers is unknown.

Since the drag was so large, the average lift-to-drag ratio of the autorotating wing was much less than for a conventional wing. The average lift-to-drag ratio increased with increasing Reynolds number and approached an asymptotic limit at 1·47. The primary cause of the low lift-to-drag ratio was the energy lost in the vortices shed periodically as the lift fluctuated. Hence, although the lift-to-drag ratio could be somewhat increased by increasing the aspect ratio and reducing the induced drag, it appears to be impossible to obtain a high lift-to-drag ratio for an autorotating wing.

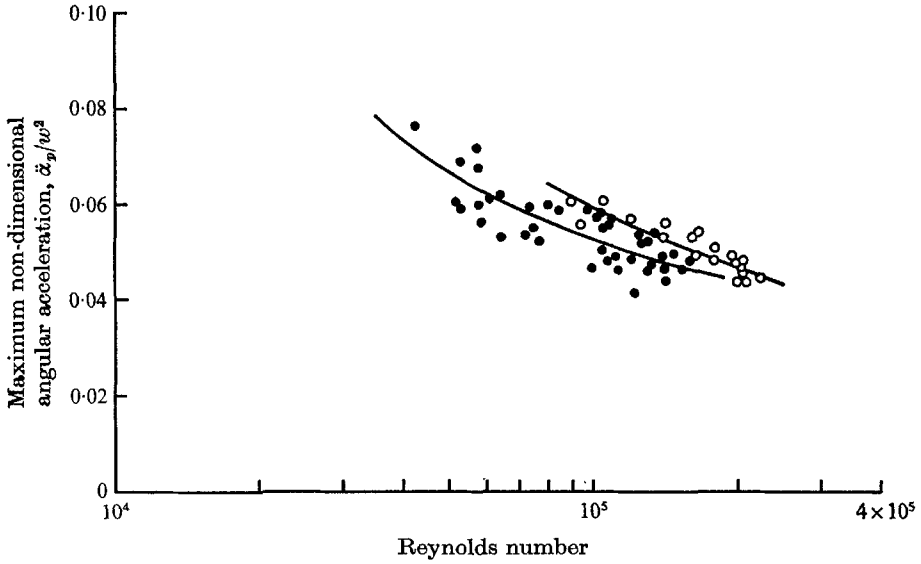

FIGURE 11. Maximum angular acceleration *vs.* Reynolds number. $I^* = 8{\cdot}47$; ○, mechanical bearings; ●, air bearings.

The maximum angular acceleration was much less than if the maximum lift force had acted through the quarter chord and corresponded to a very small fluctuation in the angular velocity of the wing. The curve of angular acceleration was nearly sinusoidal with the maximum angular acceleration at an angle of attack of about 35° and the minimum angular acceleration at an angle of attack of about −45° (see figure 6). The shape of the curve was unchanged over the range of Reynolds number tested. No shift in peak locations was observed at higher Reynolds numbers, but a small shift might not have been noticed since the signal-to-noise ratio was poorer than for the lift and drag data.

The angular acceleration $\ddot{\alpha}$ was non-dimensionalized by dividing it by the square of the wing rotation rate in radians per second, w^2. The resulting quantity, $\ddot{\alpha}/w^2$, is approximately proportional to the angular velocity fluctuation; it would be exactly proportional if the angular acceleration were shown as a function of Reynolds number in figure 11. It was small and decreased as the Reynolds number increased and followed the same trend, but was larger, when the air

bearings were replaced with mechanical bearings. The angular velocity fluctuation was calculated by integrating the angular acceleration data numerically and was only $\pm 2{\cdot}1\,\%$ at $Re = 108\,000$. Because the fluctuations in angular velocity were so small, the wing was assumed to rotate at a constant angular velocity. This greatly simplified analysis of the motion since it was then necessary to know the angular position at only one point in the cycle. The estimated maximum error in the angular position caused by the assumption of constant angular velocity was only $0{\cdot}61°$ at $Re = 108\,000$.

5. Wing rotation rate

The wing rotation rate is discussed in terms of the Strouhal number which is the non-dimensional wing rotation rate nc/U (see §3). The Strouhal number was measured over a wide range of Reynolds numbers for a 15 % thick symmetrical airfoil, which was symmetric both fore and aft and vertically (see figure 12). The Strouhal number increased when the Reynolds number increased to $Re = 7500$ for needle bearings and $Re = 13\,000$ for air bearings, then decreased to a minimum.† Following the minimum, the Strouhal number increased and approached an asymptotic limit at $S = 0{\cdot}35$.

The probable reason for the increase in the Strouhal number at higher Reynolds numbers (above the local maximum and minimum) is the later stall of the wing at higher Reynolds numbers for a given Strouhal number (see §3). Because the wing stalls later the lift pulse lasts longer and reaches a higher maximum. This increases the driving moment on the wing and, therefore, the Strouhal number. The increased Strouhal number then further increases the stalling angle, so that the lift and Strouhal number are increased still more. Thus the Strouhal number is very sensitive to changes in the Reynolds number.

The cause of the peak in the Strouhal number at $Re = 7500$ to $13\,000$ is not known, but it could be caused by transition to a turbulent boundary layer on the suction side of the wing while the flow is attached. In view of the large difference in the locations of the peak and following minimum for the needle and air bearings it would appear that the peak location is very sensitive to changes in the Strouhal number. A similar peak occurred in our tests with a flat plate airfoil; this peak also occurred earlier when the Strouhal number was reduced by increased bearing friction or a reduced I^* (as shown later).

As explained in §3, an autorotating wing must have a sufficiently high moment of inertia in order to be able to overcome the retarding torque that exists during part of its cycle. As the moment of inertia of the wing is increased the Strouhal number increases because the wing is slowed less during the stalled portion of its cycle. A wing with a lower moment of inertia does not get a corresponding gain during the unstalled portion of the cycle because its speed is limited by the flow velocity. Thus, the Strouhal number increases with increasing wing moment of inertia and approaches an asymptotic limit at which the wing would rotate at a constant angular velocity.

† A group of students working under Coles (1957) observed a similar peak at $Re = 13\,000$ for a flat plate with $I^* = 55{\cdot}6$ in fixed-axis autorotation.

The moment of inertia required for autorotation is quite low. The minimum I^* for fixed-axis autorotation was only 0·623 at $Re = 1800$ (see figure 13). For freely falling wings (see §7) the I^* required for autorotation was even less; it was 0·20 at $Re = 1800$. At $I^* = 8{\cdot}47$ the angular velocity was already almost

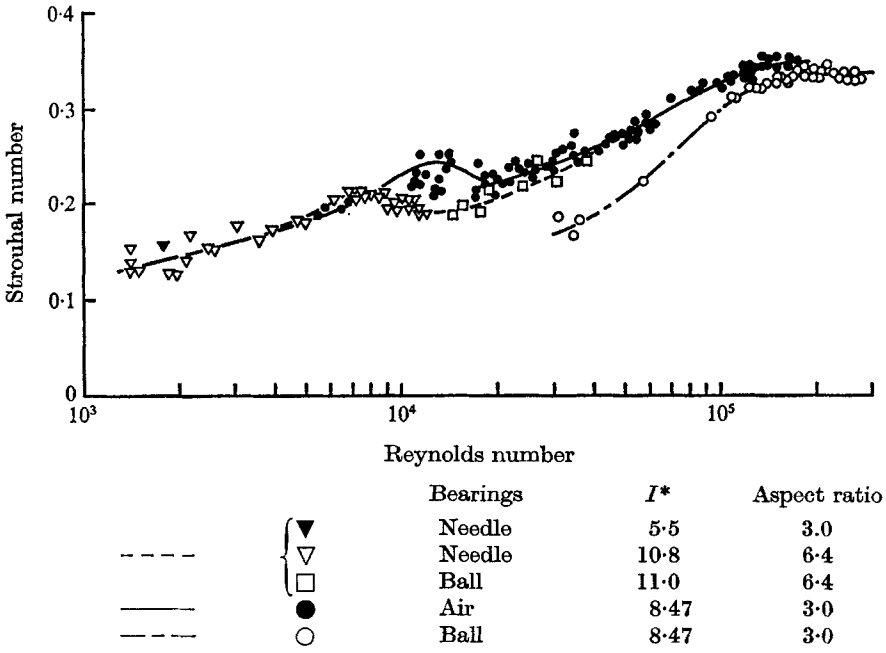

		Bearings	I^*	Aspect ratio
	▼	Needle	5·5	3.0
- - - -	▽	Needle	10·8	6·4
	□	Ball	11·0	6·4
———	●	Air	8·47	3·0
— — —	○	Ball	8·47	3·0

FIGURE 12. Strouhal number *vs.* Reynolds number for an elliptical airfoil.

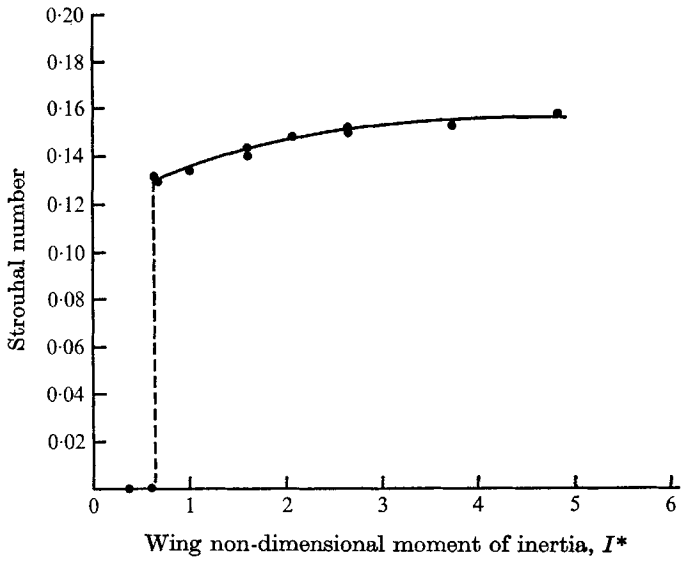

FIGURE 13. Influence of I^* on Strouhal number for an elliptical airfoil, using needle bearings, $A = 3{\cdot}0$, $Re = 1880$.

constant, with only a $\pm 2{\cdot}1\,\%$ fluctuation at $Re = 108\,000$ for fixed-axis autorotation. Hence the Strouhal number is probably nearly independent of I^* for I^* greater than ten.

The centre of gravity location may also be important, especially if the wing is rotating about a horizontal axis or is freely falling (see §7). However, no attempt was made to study this.

6. Autorotation with retarding torque

As explained in §3, when an autorotating wing is started it experiences a large net driving torque. This increases its angular velocity until the average torque is reduced to zero by aerodynamic damping. Hence a wing can autorotate more slowly than its free autorotation rate and extract energy from the air in the manner of a windmill. As the torque is increased the rotation rate decreases. Eventually, at a sufficiently high retarding torque, the wing is no longer able to pass through the stalled portion of its cycle and autorotation ceases.

To study this phenomenon the wing was fitted with a pulley and allowed to raise a weight hanging on a thread wrapped around the pulley. The Strouhal number decreased monotonically with increasing retarding torque and was very sensitive to retarding torque at low torques. Hence, even a small amount of bearing friction would appreciably slow the wing, as was observed when the air bearings were replaced with ball bearings (see figure 12).

The lift and drag also decreased monotonically with increasing retarding torque. However, they were much less sensitive than the Strouhal number. At the maximum torque at which the wing would autorotate the maximum lift coefficient was 0·55 of its value with no torque and the maximum drag coefficient was 0·83 of its value with no torque (at $Re = 61\,000$). In contrast, the Strouhal number was only 0·216 of its value with no torque at the maximum torque at which autorotation was possible.

The power output from the wing was obtained by multiplying the retarding torque and the wing rotation rate. It was then non-dimensionalized by dividing it by $1/2\rho U^3 s$, where U is the free-stream velocity and s the wing area, to yield the power coefficient. The torque coefficient was similarly obtained by dividing the retarding torque by $1/2\rho U^2 sc$ (see figure 14). As the retarding torque was increased the power coefficient increased until it reached a maximum. Then, the decreasing Strouhal number began to outweigh the increasing torque and the power coefficient decreased. The power coefficient increased at higher Reynolds numbers because the Strouhal number was higher for a given torque coefficient.

The maximum power coefficient was 0·094 at $Re = 94\,500$; Marks (1941) gives 0·145 to 0·425 for various types of windmills.† Although the power coefficients for the autorotating wing increased at higher Reynolds numbers it seems doubtful whether an autorotating wing would ever be as efficient as a well-designed windmill.

Since reducing the Strouhal number of the wing reduced the maximum and

† The power coefficient for a windmill is based on the disk area; for the autorotating wing it is based on the wing area.

average lift and drag it seemed probable that increasing the Strouhal number should increase them. This was found to be true, but detailed measurements were not made because the apparatus did not allow sufficient running time. Foshag & Boshler (1969) have collected a large amount of experimental data by various investigators for both free and powered autorotation. For example, Küchemann (1942) measured a lift coefficient of twelve with a drag coefficient of about eight, at a Strouhal number of 2·46.

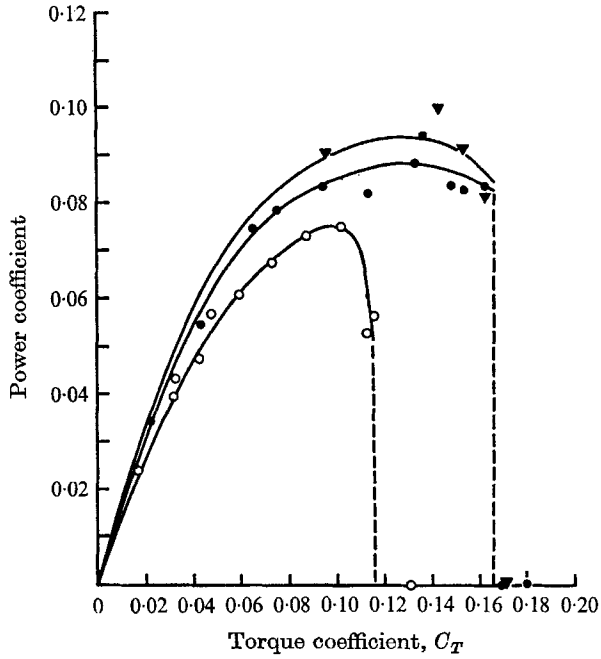

FIGURE 14. Power output of autorotating wing. ○, Re = 23 000; ●, Re = 61 000; ▼, Re = 93 500.

7. Freely falling autorotation (Tumbling)

All of the preceding data has been for a wing autorotating about a fixed axis. However, a freely falling wing can also autorotate. The motion of a freely falling wing differs from that of a wing autorotating about a fixed axis in that it has six degrees of freedom instead of one. The problem can be simplified if the wing is assumed not to side-slip and the spanwise axis of rotation is assumed not to rotate about a horizontal or vertical axis. This means that the motion is two-dimensional and reduces the number of degrees of freedom to three. Two-dimensional motion is observed for a large aspect ratio wing autorotating in a stable manner. The two additional degrees of freedom allow the wing to rise and fall about its average path and to change speed along its path, in effect changing the free-stream velocity and Strouhal number. There is, of course, a coupling between the wing motion and the forces causing it.

A group of students working under Coles (1957) studied the motion of falling

autorotating wings by photographing their flight. A strobe lamp flashed every 1/180 second and provided a series of images that showed the path and angular position as a function of time. They found that the lift-to-drag ratio increased from 0·78 for an aspect ratio of 1·13 to 1·40 for an aspect ratio of nine. The average lift coefficient (based on the average velocity of the wing along its path) was 1·69 for an aspect ratio of nine.

Our work also included some tests with falling wings. The results were similar to those of Coles (1957) but the lift-to-drag ratios and average lift coefficients were somewhat higher for a given aspect ratio. A wing with an aspect ratio of 1·33 had a lift-to-drag ratio of 1·24 and an average lift coefficient of 1·61 (again, based on its average speed along its path). For a wing with an aspect ratio of four, the lift-to-drag ratio was 1·58 and the average lift coefficient was 2·09.

Our tests probably gave higher lift-to-drag ratios and average lift coefficients because the wings had larger tip plates and higher Reynolds numbers. Our wings had 1·33 chord diameter tip plates and Reynolds numbers of about 10000, compared with 1·0 chord diameter tip plates and Reynolds numbers of about 4500 for the tests of Coles. The I^* were also different, $I^* = 9{\cdot}0$ in our tests and $I^* = 4{\cdot}0$ in Coles's tests, but the effect of this difference was probably small. The influence of I^* on the lift-to-drag ratio and average lift coefficient was not studied in detail but no large changes were observed for even very large changes in I^* provided I^* was greater than one.

In all the tests described previously, for both freely falling and fixed-axis autorotation, the airfoils used were symmetric both fore and aft and vertically. It seemed possible that a properly cambered airfoil might gave substantially more lift. To investigate this, an S-shaped airfoil formed from two circular arcs of 1·0 chord radius was built. This did give a higher Strouhal number for both fixed-axis and freely falling autorotation, but in freely falling autorotation the lift-to-drag ratio was increased only 6 % and the average lift coefficient was not significantly changed. When the wing was rotated against its camber (i.e. with the forward half of the wing cambered negatively) the Strouhal number decreased to well below that obtained with a flat plate. However the lift-to-drag ratio decreased only 8 % and the average lift coefficient was still almost unchanged. Hence, it appears that a cambered wing offers no advantages except that it has a preferred direction of rotation. A camber of 0·5 chord radius was sufficient to ensure that the wing would always rotate toward its camber regardless of how it was dropped or initially spun.

The photographs of the path of a falling wing taken by Coles showed that the motion was quite similar to that of a fixed-axis autorotating wing viewed from a reference point moving at the free-stream velocity. In a test with $I^* = 4{\cdot}0$ and an aspect ratio of nine, the maximum deviation of the wing from its mean path was about 0·05 chord with the maximum slope of the path relative to the mean path about 10°. The maximum fluctuation in velocity along the path was only ± 10 % and the fluctuation in angular velocity was $\pm 6{\cdot}7$ %, comparable to that observed in fixed-axis autorotation. The lift-to-drag ratio and average lift coefficient were also comparable to those for fixed-axis autorotation. Thus, it appears that the autorotation phenomenon is basically the same for both

freely falling and fixed-axis autorotation and the flow patterns are probably similar, at least for wings with I^* high enough to ensure reasonably continuous rotation.

For sufficiently low Reynolds numbers or I^*, falling wings did not autorotate but fell in a stable manner or with a rocking motion (see figure 15). For Reynolds numbers less than 50–85, depending on I^*, the wings fell steadily perpendicular to their path without any periodic motion and would move to a position perpendicular to their path if dropped in some other position.† For higher Reynolds

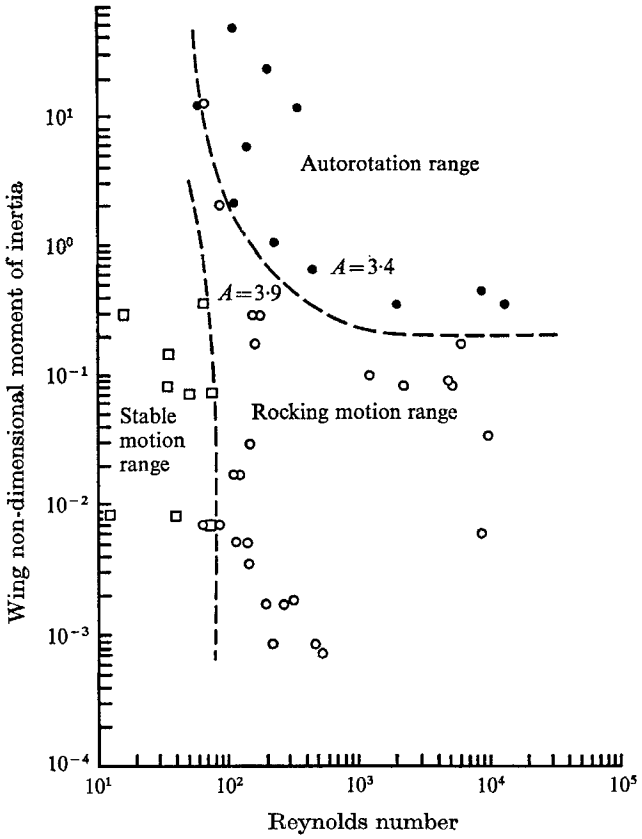

FIGURE 15. Range of I^* and Reynolds number for various types of motion of a falling wing.

numbers the wings fell with a slight rocking motion that became more severe as the Reynolds number was increased. At sufficiently high Reynolds numbers, and I^*, the wings began to autorotate. For I^* less than 0·10, the wings did not autorotate even at high Reynolds numbers but the oscillations became a periodic gliding type of motion with large horizontal displacements.

The flow pattern was not studied but this is well discussed by Willmarth,

† Willmarth, Hawk & Harvey (1964) report that for Reynolds numbers less than one a body with three mutually perpendicular planes of symmetry will not orient itself but will remain in its initial position.

et al. (1964) for falling disks, which behave in the same manner and probably have very similar flow patterns. The basic mechanism is that for sufficiently low Reynolds numbers, the wake behind the disk or wing being stable with no periodic vortex shedding and, therefore, no pitching moments on the model. As the Reynolds number increases, the wake becomes unstable and the model begins to oscillate and to shed periodic vortices. At higher Reynolds numbers the vortex shedding and oscillations are more violent and for high enough Reynolds numbers and I^* the model oscillates more and more violently until it overturns and begins to autorotate.

The boundary locations for the three types of motion were similar for the disk and flat plate except that the flat plate required a much higher I^* to autorotate for a given Reynolds number. The reason why the flat plate required a higher I^* for autorotation was probably that the disk could autorotate without turning directly over. That is, as the disk rotated to an angle of attack of perhaps 45°, the axis of rotation rotated to an angle to the horizontal and the disk completed its cycle by sliding off sideways. This produces a very random tumbling motion as observed by Willmarth *et al.* (1964). In contrast, a rectangular plate with an aspect ratio much greater than one cannot do this readily because of the stabilizing effect of the large aspect ratio. Therefore it must rotate directly over, which requires more angular momentum.

8. Conclusions

In the first six sections of this paper, the behaviour of a fixed-axis autorotating wing has been discussed in detail, as a function of Reynolds number. Most of the discussion has centred on one wing configuration, as described in §2. However, the Strouhal number was measured for a variety of symmetrical and unsymmetrical airfoils, aspect ratios from 1·33 to 6·42, and a number of tip plate configurations. Also, spanwise fences of various heights were mounted on the instrumented wing at various positions along the chord and the maximum lift coefficient and Strouhal number were measured. The flow pattern was studied for the instrumented wing, both with and without spanwise fences, and for flat plates of two aspect ratios.

Except for spanwise fences which were so large† that they prevented autorotation, none of these changes had a major effect on the gross properties of the autorotation phenomenon. Although the Strouhal number and lift and drag coefficients changed they were always of the same magnitude and the flow pattern exhibited the same basic behaviour for all of the configurations for which it was studied. Also, for comparable Reynolds numbers freely falling wings behaved basically in the same manner as was observed for fixed-axis autorotating wings. Thus, it would appear that the general conclusions reached in this paper are probably valid for any autorotating wing operating at comparable Reynolds numbers and Mach numbers well below one.

† Fences 0·25 chord high, mounted at the mid-chord on both sides of the wing.

The author would like to acknowledge the valuable help of Dr William W. Willmarth, who was the chairman of his doctoral committee and also the financial support of the United States Army, under AROD Contract DAHCO–4–68C–0027.

REFERENCES

AHLBORN, F. 1897 Der Schwebflug und die Fallbewegung Ebener Tafeln in der Luft. *Abh. Naturw. Ver., Hamburg*, **15**.

COLES, D. 1957 Tumbling airfoil. Unpublished student project, Graduate Aeronautical Laboratory, California Institute of Technology.

ERICSSON, L. E. & REDING, L. P. 1969 Unsteady airfoil stall. *N.A.S.A.* CR 66787, 19.

FOSHAG, W, F. & BOSHLEV, G. D. 1969 Preview and preliminary evaluation of lifting horizontal axis rotating-wing aeronautical systems (HARWAS). *U.S. Army Aviation Material Lab. Tech. Rep.* no. 69–13.

HAM, N. D. 1968 Aerodynamic loading of a two-dimensional airfoil during dynamic stall. *A.I.A.A. J.* **6**, 1927–1934.

HOERNER, S. F. 1965 *Fluid Dynamic Drag*, pp. 7–10. Published by author, 148 Busteed Drive, Midland Park, New Jersey.

KÜCHEMANN, D. 1942 Auftrieb and Widerstand eines Rotierenden Flugeln. *Deutsche Luftfahr-Forschung, Aerodynamische Versuchsantalt, Göttingen*, no. FB-1651, 8.

MARKS, L. S. 1941 *Mechanical Engineer's Handbook*, 4th ed., p. 1133. McGraw-Hill.

MASKELL, E. C. 1963 A theory of the blockage effects on bluff bodies and stalled wings in a closed wind tunnel. *Aero. Res. Counc. R. & M.* no. 3400.

POPE, A. & HARPER, J. 1966 *Low Speed Wind Tunnel Testing*, pp. 326–32. New York: Wiley.

SMITH, A. M. O. 1953 On the motion of a tumbling body. *J. Aeron. Sci.* **20**, 73–84.

WILLMARTH, W. W., HAWK, N. E. & HARVEY, R. L. 1964 Steady and unsteady motions and wakes of freely falling disks. *Phys. Fluids*, **7**, 197–208.